Available online at www.sciencedirect.com
ScienceDirect
Journal of Power Sources 173 (2007) 531–537
JOURNAL OF POWER SOURCES
www.elsevier.com/locate/jpowsour

Spectroscopic and electrochemical characterization of the passive layer formed on lithium in gel polymer electrolytes containing propylene carbonate

Hu Cheng, Changbao Zhu, Mi Lu, Yong Yang *

State Key Laboratory for Physical Chemistry of Solid Surface, Department of Chemistry, Xiamen University, Xiamen 361005, PR China

Received 28 September 2006; received in revised form 8 April 2007; accepted 11 April 2007
Available online 22 April 2007

Abstract

The passive layer formed on lithium in a PEO_{20}–LiTFSI–5%PC gel polymer electrolyte after different electrochemical processes was characterized using X-ray photoelectron spectroscopy (XPS), Fourier transform infrared spectroscopy (FTIR), and electrochemical impedance spectroscopy (EIS). EIS indicates that the interface resistance of lithium electrodes increases with time after fresh lithium deposition, whereas the interfacial resistance has no change with time after lithium deposition/dissolution process. The XPS analysis as well as FTIR data show that the main compositions of the passive layer are $ROCO_2Li$, Li_2CO_3, LiOH, LiX (X = F, S, N, SO_2CF_3) and Li oxides, mostly due to the reactions occurred between lithium and PC, LiTFSI, and trace impurities (H_2O, O_2), and the lithium dissolution process has no distinctive effect on the composition of passive layer. XPS depth profile of the passive film detected by XPS and sputtering experiments further demonstrates that the presence of Li_2CO_3/LiOH is in the outer layer and Li_2O, LiF mainly in the inner part of the passive layer.

Keywords: XPS; FTIR; Polymer electrolyte; Passive layer; Nickel; Lithium

1. Introduction

Recently, lithium polymer electrolyte batteries are receiving much attention because they offer a number of significant advantages both in terms of high energy density and good safety performance. However, there are many problems to be resolved in these systems. One problem is the formation of a passive layer at the lithium/polymer electrolyte interface where in many cases this layer becomes more and more impervious to ion conduction and results in poor performance of the battery. Therefore, it is crucial to have a good understanding of the passive layer in developing advanced lithium batteries.

There have been various studies on the formation of passive layers between lithium electrode and polymer electrolytes by using electrochemical and ex situ spectroscopic techniques [1–13]. It is generally accepted that in polymer electrolyte systems, lithium is covered by a passive layer and the resistance of this layer grows with time until it is larger than the bulk resistance. From an electrochemical point of view, the formation of a passive layer at the interface of lithium/polymer electrolyte systems is usually considered similar to lithium in liquid organic electrolyte. The major differences between these two systems result from the physical stiffness of the polymer electrolytes. Polymer electrolytes are either hard-to-soft solids, or a combination of solid and molten phases in equilibrium. As a result, wetting and contact problems must be considered at the lithium/polymer electrolyte interface. Therefore, the passive layer at the lithium/polymer electrolyte interface should be thin and inhomogeneous.

In previous publications, the composition and structure of the passive layers in lithium-liquid systems have been well characterized, mainly using XPS [4–7], FTIR [8,9], Raman [10], SIMS [11,12], TPD-MS [13]. These techniques can provide some ex situ information. However, there have been very few reports to deeply study of the composition and structure at the lithium/polymer electrolyte interface by above spectroscopic methods [14,15].

* Corresponding author. Tel.: +86 592 2185753; fax: +86 592 2185753.
E-mail address: yyang@xmu.edu.cn (Y. Yang).

0378-7753/$ – see front matter © 2007 Published by Elsevier B.V.
doi:10.1016/j.jpowsour.2007.04.027

In general, polymer electrolytes could be roughly divided into two major classifications: (1) solid polymer electrolytes (SPEs), and (2) gel polymer electrolytes (GPEs). Compared with the former, GPEs are more promising systems because of their inherited higher ion conduction which is due to the presence of the small organic molecules. However, the compatibility of GPEs with lithium metal must be enhanced, which means that a stable, low impedance passive layer should be formed. Therefore, in this work, by EIS, XPS, and FTIR we have investigated resistance and composition of the passive layer formed on lithium in a gel electrolyte system which was electrodeposited on a nickel substrate. As nickel metal does not form alloys with lithium, we can explore fundamental aspects of Li electrodeposition without complications derived from the formation of other phases [16]. We present a careful analysis of XPS measurements as well as supporting FTIR data, and propose the formation mechanism and models for the passive layer on Li electrode in PC-containing gel electrolytes mainly based on our results.

2. Experimental

2.1. Materials and preparation

PEO (M_w = 600,000, Aldrich) and LiTFSI (Aldrich) were dried under high vacuum for 48 h at 100 °C before use. PC (Aldrich) was purified by distillation under vacuum. Polymer electrolyte was prepared by solution casting. PEO, LiTFSI and PC were mixed in the appropriate ratios (MO/Li: 20, PC: 5%) with acetonitrile (HPLC, Shanghai Reagent) and stirred vigorously for 48 h until a homogenous solution was formed. The viscous solution was cast into a polytetrafluoroethylene (PTFE) mold and evaporated with a 4 Å molecular sieve as an absorber at room temperature. Flexible polymer electrolyte membranes (PEO_{20}–LiTFSI–5%PC) were stored in a glove box (Labmaster, Mbraun Co.) under argon atmosphere and then used in electrochemical measurements followed by XPS and FTIR analyses.

2.2. Electrochemical measurements

Electrochemical measurements were performed in three-electrodes cell, using nickel metal as working electrode and metallic lithium as both the counter and reference electrodes whose native surface film was scraped off before assembling. The polymer electrolyte was placed between working electrode and counter electrode, forming a thin layer cell. The assembling procedure was carried out in the glove box. The electrochemical measurements were performed by using an autolab PGSTAT30 electrochemical instrument (Metrohm Co.). Two different procedures were used: (1) the cell was cycled in the range from −0.5 to +2.0 V and the process of the deposition and dissolution of lithium happened on a nickel substrate, and (2) the cell was reduced down to −0.2 V and lithium was electrodeposited on a nickel substrate.

2.3. XPS measurements

After electrochemical measurements, the cell was disassembled in a glove box under argon atmosphere. The polymer electrolyte membrane was carefully peeled off from the nickel substrate, and then the nickel substrate was mounted on an XPS stage using conductive carbon adhesive tape. To avoid any sample from moisture/air exposure, the XPS stage was placed in a hermetic vessel and transferred to the instrument in the dry nitrogen atmosphere. XPS measurements were performed on a PHI Quantum 2000 Scanning ESCA Microprobe with a monochromatic Al $K\alpha_{1,2}$ radiation (1486.6 eV). The diameter of the monitoring point is 200 μm. Survey scan spectra were acquired at 187.85 eV pass energy and narrow scan spectra were acquired at 58.70 eV pass energy. The instrument vacuum was maintained at $\sim 5 \times 10^{-7}$ Pa. Sputtering experiments were performed using an argon ion beam gun operating at 4 kV, and the sputtering rate was roughly estimated to be 1.5 nm s^{-1} calibrated for SiO_2. The binding energy for each spectrum for Ni surface was calibrated by C 1s peak, corresponding to hydrocarbon absorbed on the sample surface (284.8 eV). Peak fitting was performed using the XPSPEAK software.

2.4. FTIR measurements

FTIR spectra were acquired on a Nicolet avatar 360 FTIR spectrometer (Thermo Nicolet Co.) in the range of 4000–400 cm^{-1} with a resolution of 4 cm^{-1} using Omnic 6.0a software. The samples were obtained by scraping the passive layer from the nickel substrate with a knife after electrochemical measurements and pressed into KBr pellets in a glove box. Dry nitrogen was used to protect the sample surface from reaction with the atmosphere.

3. Results and discussion

3.1. Electrochemical investigation

Fig. 1 shows the first cyclic voltammogram and partial enlarged detail (0.7–2.0 V) of the clean nickel electrode in PEO_{20}–LiTFSI–5%PC electrolyte recorded at 323 K from −0.5 to 2.0 V versus Li/Li^+ at a scan rate of 0.3 mV s^{-1}. The peaks in the cathodic direction between 1.4 and 2.0 V were ascribed

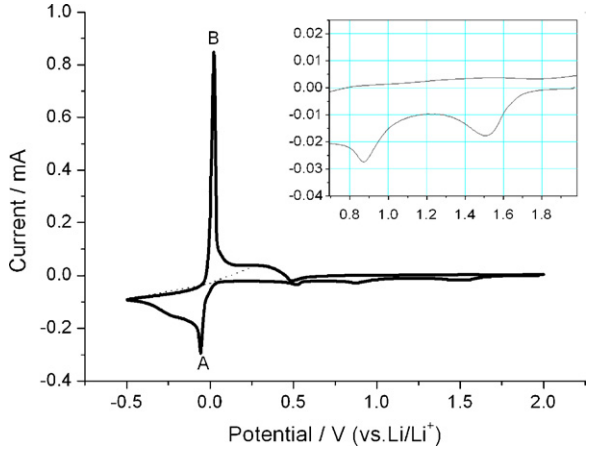

Fig. 1. First cyclic voltammogram for nickel in PEO_{20}–LiTFSI–5%PC in the range −0.5 to +2.0 V vs. Li[C/R] at 323 K. Scan rate: 0.3 mV s^{-1}.

to the reduction of trace oxygen and water in the polymer electrolyte, and the products are LiOH and Li oxides [16,17]. The presence of these products has been proved by the following XPS and FTIR analysis. The peak observed between 0.8 and 1.0 V in the cathodic direction may be attributed to the under-potential deposition (UPD) of Li on Ni [16,17]. The pronounced peaks: A (−0.06 V) and B (0.02 V), are due to Li bulk deposition and dissolution, respectively. Because the contacting area between electrode and polymer electrolyte is not accurately known, due to the difficulties in placing the two electrodes perfectly parallel to each other, it is not possible to determine reliably the charge density. However, an estimation of the area of electrochemical contact could be made after Li bulk deposition. For this cell, the value of electrochemical active surface area was about 1 cm^2. Therefore, without considering surface roughness, the charge densities calculated from peaks A and B, using the dotted lines as baselines, are ca. 126.4 mC cm^{-2} for the deposition and ca. 106.6 mC cm^{-2} for the dissolution. These indicate that the electrochemically active lithium on the nickel substrate was mostly removed after Li deposition–dissolution cycle.

Fig. 2 shows Nyquist plots of the ac impedance data obtained from nickel electrodes after different electrochemical measurements in PEO_{20}–LiTFSI–5%PC electrolyte at 323 K. It is obvious that there is an arc appearing in the middle high frequency both after cycle and after deposition. The arc is generally attributed to the formation of a passive layer [18,19]. It should be noted that the interface resistance after Li deposition increases with time, whereas the interfacial resistance after Li deposition–dissolution cycle is constant for a long time, due to the existence of the active lithium thin film on the electrode.

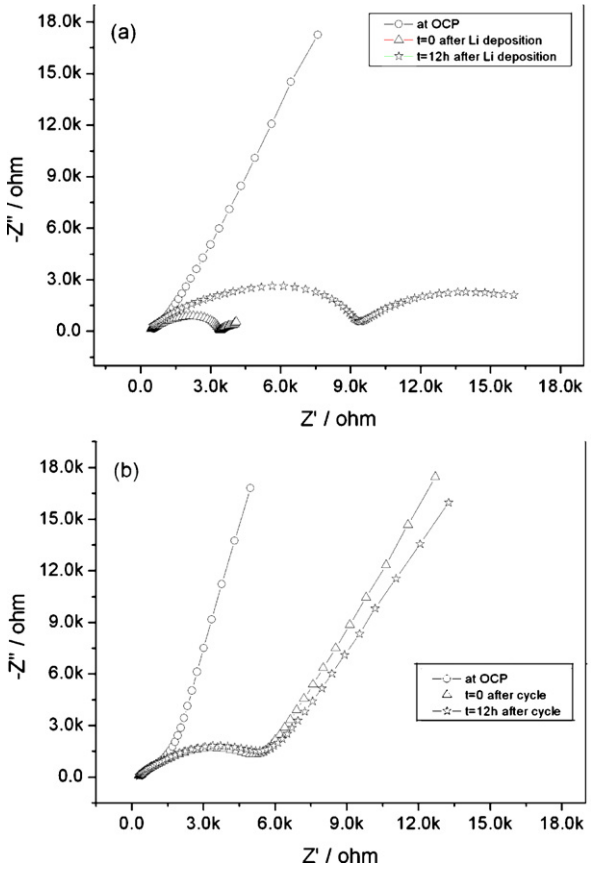

Fig. 2. Nyquist plots obtained from nickel substrate electrodes: (a) after Li deposition and (b) after Li deposition–dissolution cycle in PEO_{20}–LiTFSI–5%PC electrolyte at 323 K.

3.2. XPS analysis of the passive layer on the lithium electrodes

Two electrodes were recovered from two different electrochemical cells as described above. Lithium which was electrodeposited on the electrode bears the electrochemically activity and probably reacts with each component in polymer electrolyte.

Lithium electrodes in pure PC solution or liquid electrolyte containing PC have been already intensively studied [20], but there are few investigations on the effect of small amount of PC in polymer electrolyte on the passive layer formed on lithium, and whether the PC molecules can play an important role in the formation of passive films should be an interesting topic. Fig. 3 presents the C 1s and O 1s XPS spectra measured from the electrodes after cycle and deposition. The experiments included Ar^+ sputtering followed by XPS measurements. Each spectrum was treated by the deconvolution software to account for the different oxidation states of the elements. The C 1s spectra obtained from two samples before and after sputtering contain several carbon peaks of 283–284, 284–285, 286–287, 288–289, and 290–291 eV. The peak at 284.8 eV is attributed not only to hydrocarbon contamination (always existed in the glove box and/or the XPS chamber and mainly adsorbed on the outer surface of the sample) but also to carbon atoms of C–C or C–H in possible organic species. The shoulder peak at 286.5 eV is attributed to carbon atoms of C–O, and it is likely to the methyl carbon in $ROCO_2Li$ [21]. The peak at 290.4 eV is assigned to the carbon bound to the three oxygen atoms in the carbonate species (both Li_2CO_3 and $ROCO_2Li$). The peak at 288.6 eV suggested the presence of a species with C=O character, possibly an ester. Then we can also find several peaks corresponding to $ROCO_2Li$ at 532.8eV, Li_2CO_3/LiOH at 531.4 eV, Li_2O at 528.2 eV from the O 1s spectra.

From the chemical stability point of view, PEO is considered to be rather inert to lithium than PC. However, Teeters still proposed that lithium possibly breaks the polymer chain at the C–O bond to form LiOR type compounds [22]. In our experimental data, we do not find the clear evidence for the chemical reaction of lithium with PEO itself. Therefore, the above results mainly show that PC is reduced on lithium to a $ROCO_2Li$ species containing carbonate groups (C 1s peak at 290.4 eV and O 1s 532.8 eV) and alkyl groups (C 1s peak around 286–287 eV). Such $ROCO_2Li$ species have been widely described as the main components of the passive layers forming on various electrodes, such as lithium, graphite, and metal oxides [4,23]. However, in our results, these peaks at 290 eV in the C 1s spectra and at 531.4 eV in the O 1s spectra indicated that Li_2CO_3 is the dominant species in the passive layer. The reason is that $ROCO_2Li$ can further react with trace water in the electrolyte to form Li_2CO_3.

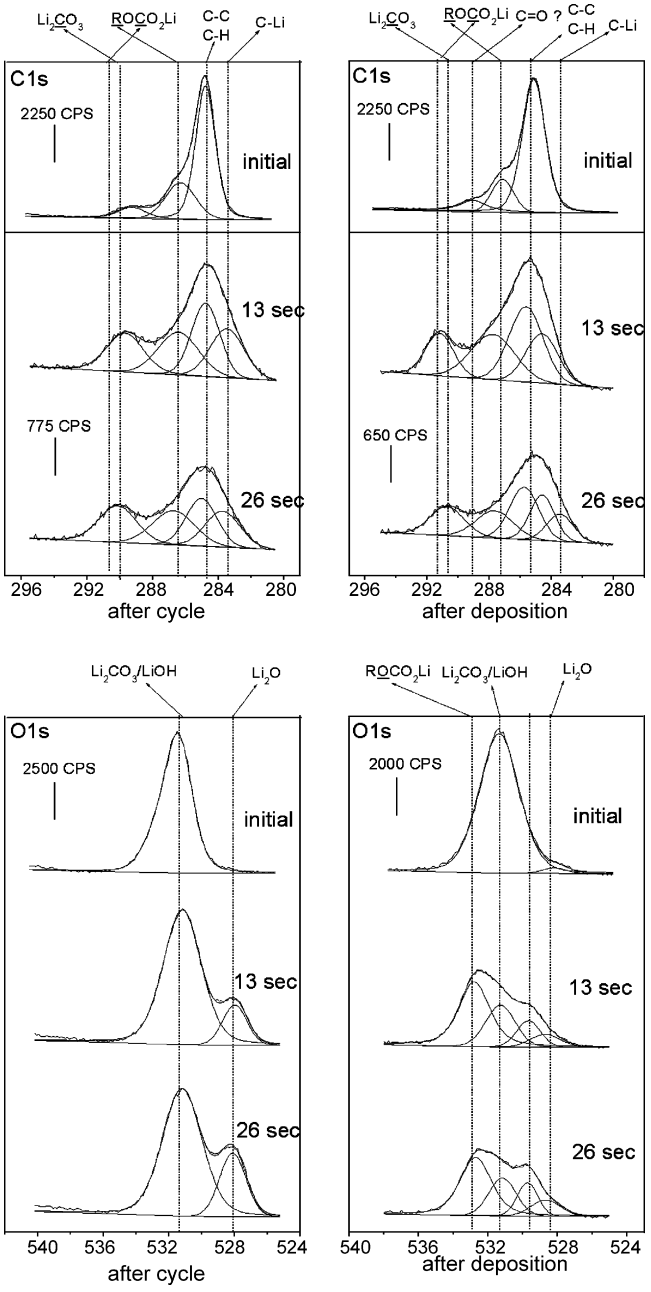

Fig. 3. C 1s and O 1s XPS spectra and their fit curve for the nickel substrate in the PEO_{20}–LiTFSI–5%PC electrolyte before and after sputtering.

Scheme 1 presents the simple reduction pattern of PC on lithium [4].

Fig. 4 presents the XPS spectra of Li 1s, F 1s, N 1s and S 2p regions measured from the electrodes after Li deposition–dissolution cycle and Li deposition. The experiments included Ar^+ sputtering followed XPS measurements. Each spectrum was treated by the deconvolution software to account for the different oxidation states of the elements. In any

$$2PC + 2Li^+ + 2e^- \rightarrow CH_3CH(OCO_2Li)CH_2OCO_2Li + CH_3CH{=}CH_{2(g)}$$
$$CH_3CH(OCO_2Li)CH_2OCO_2Li + H_2O \rightarrow Li_2CO_3 + CH_3CH(OH)CH_2OH$$

Scheme 1. Two reduction routes of PC on lithium electrodes [4].

$$LiN(SO_2CF_3)_2 + ne^- + nLi^+ \rightarrow Li_3N + Li_2S + Li_2O + LiF + C_2F_xLi_y$$
$$LiN(SO_2CF_3)_2 + 2e^- + 2Li^+ \rightarrow Li_2NSO_2CF_3 + LiSO_2CF_3$$

Scheme 2. Two reduction routes of LiTFSI on lithium electrodes [24].

case, these spectra basically displayed similar feature. In the F 1s region spectrum, peaks were identified for SO_2CF_3 at 689.9 eV and LiF at 684.8 eV. The S 2p region spectrum includes a broad peak around 168 eV which is attributed to SO_2CF_3 species. A number of S 2p peaks around 160–164 eV most likely associated with elemental sulful and sulfide species (possibly Li_2S). The Li 1s spectrum appears as a broad peak centered around 54–55 eV, which is in fact a superposition of peaks attributed to LiF (56 eV), Li_2CO_3/LiOH (55.3 eV), and Li_2O (54.0 eV). The N 1s spectrum displayed a weak peak at 398.3 eV and indicated that the passive layer also contained a small quantity of nitride species (possibly Li_3N) [23].

Thus these findings suggest that LiTFSI was probably reduced on lithium to a mixture containing SO_2CF_3, LiF, Li_2S, Li_3N. Scheme 2 presents two reduction routes of LiTFSI on lithium [23].

3.3. Depth profiles of the passive layer on the lithium electrodes

Table 1 shows the peak position for deconvoluted peaks in element spectra, obtained from the two samples before and after sputtering. In the C 1s spectra (Fig. 3), it should be noted that the C 1s spectra obtained after sputtering always contain a peak around 283.3 eV. This peak, which reflects carbon at a very low oxidation state, can be attributed only to species containing C–Li bonds (carbides), probably due to the induction of sputtering [4]. Moreover, there was a slight difference between the two samples, the carbonate carbon peak obtained after cycle was shifted to lower binding energy (289.7 eV). In general, the carbonate carbon peak of $ROCO_2Li$ should appear at a higher binding energy than that of Li_2CO_3. We can thus conclude that the amount of $ROCO_2Li$ obtained after deposition is more than that obtained after cycle, and it is close to the lithium surface. From the O 1s spectra (Fig. 2) obtained after deposition, we can also find the same change. Upon sputtering, Li_2CO_3/LiOH peak decreased and Li_2O peak appeared and increased gradually. The results indicate that the presence of Li_2CO_3/LiOH is in the outer layer and Li_2O, LiF mainly in the inner part of the surface film.

In the F 1s and S 2p spectra (Fig. 4), the amount of SO_2CF_3 decreased or disappeared completely with sputtering time. On the contrary, the quantity of LiF and Li_2S increased with sputtering time. The above observations and discussion of the lithium passive layer obtained after cycle and deposition are summarized schematically in Fig. 5.

3.4. FTIR analysis of the passive layer on the lithium electrodes

XPS of the electrodes during different electrochemical process in gel polymer electrolytes is rather limited to provide a clear identification of the passive layer. Therefore, correlation

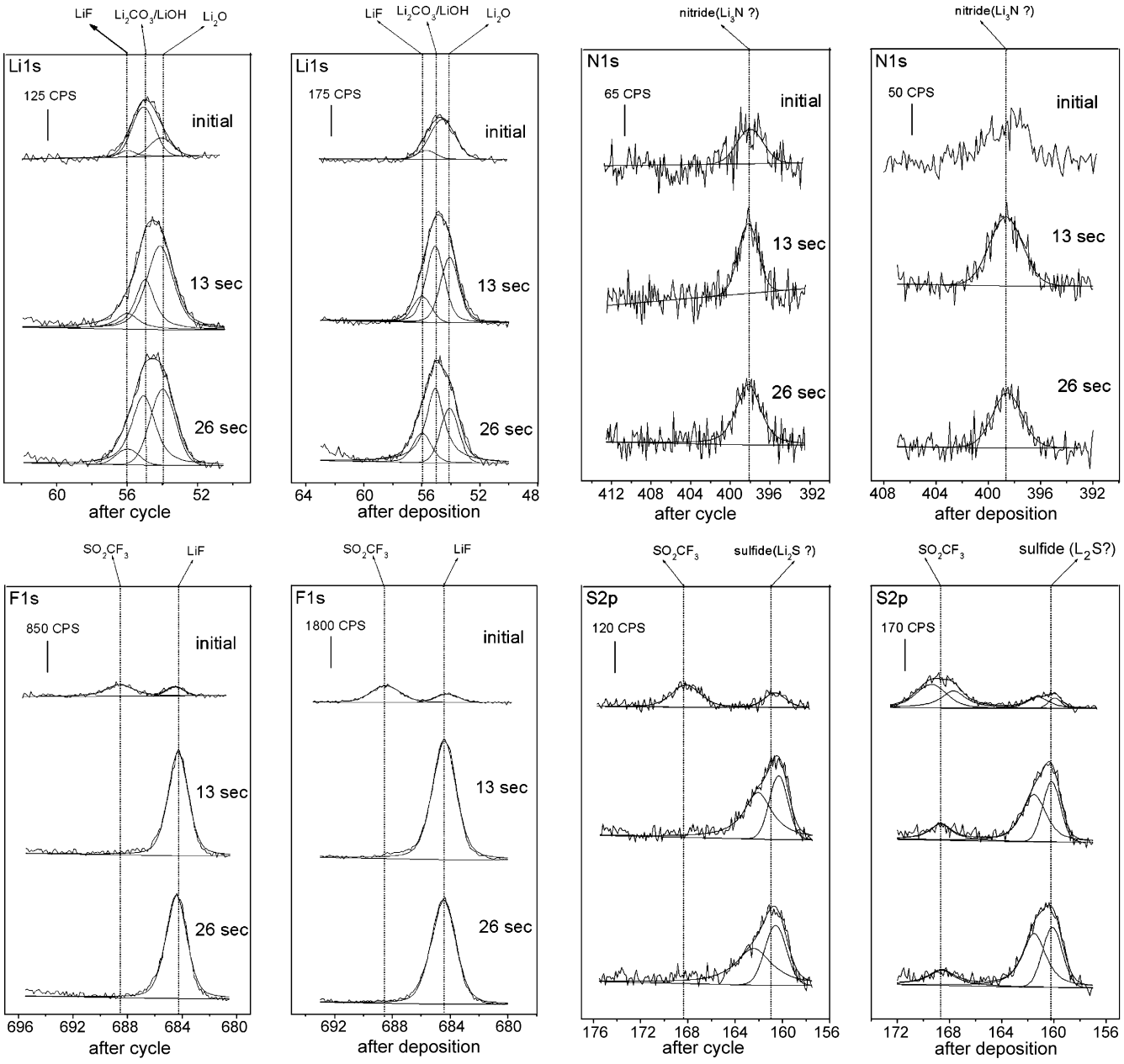

Fig. 4. Li 1s, N 1s, F 1s, and S 2p XPS spectra and their fit curve for the nickel substrate in the PEO_{20}–LiTFSI–5%PC electrolyte before and after sputtering.

of XPS data with the results obtained from FTIR spectroscopy is important. Fig. 6 presents comparative spectra obtained from the electrodes after Li deposition–dissolution cycle and Li deposition in PEO_{20}–LiTFSI–5%PC electrolyte. Table 2 shows the FTIR spectrum peak positions and their assignments. From the peak assignments we were able to observe quite clearly the existence of surface species. The spectrum features of surface films obtained from the two conditions are very similar. In detail, the peaks appeared at around 2920, 2860, 1660, 1030, 1100, 840 and 510 cm^{-1} are typical absorption peaks of $ROCO_2Li$ species. We could conclude that $ROCO_2Li$ may be the reduction product of PC. The dominant IR active component of the passive film, however, cannot be rigorously identified as any kind of lithium alkyl carbonate due to the complexity of the possible chemical and electrochemical reaction. The alkyl groups may include aliphatic, olefinic, and possibly polymeric species. This needs to be confirmed by more evidence. $ROCO_2Li$ can further react with trace water in this electrolyte and form an amount of Li_2CO_3. The presence of Li_2CO_3 peaks at 1510, 1443, 872 cm^{-1} is also examined, supporting the secondary reaction during formation of passive layers [24–26]. The passive layer also contains a few LiOH species corresponding to 3675 cm^{-1}. These are in agreement with the result mentioned above. In the XPS results we assumed the possible decomposition reaction of LiTFSI. But in our FTIR experiments we can only find some weak peaks at around 1338 and 1193 cm^{-1} related to SO_2CF_3 species. Because of the limitation of FTIR technique and the low reaction extent, we cannot acquire more evidence for the reduction reaction of LiTFSI on lithium.

Table 1
Peak position for deconvoluted peaks in element spectra, obtained from the lithium passive layer after Li deposition–dissolution cycle and Li deposition

Peak	BE (eV)					
	After cycle			After deposition		
	Initial	13 s	26 s	Initial	13 s	26 s
C 1s		283.4	283.5			283.4
	284.7	284.8	285.0	284.8	285.0	285.1
	286.4	286.5	286.7	287.1	287.6	287.7
	289.5	289.8	290.2	288.5	291.0	290.8
					532.8	532.8
O 1s	531.4	531.3	531.3	531.4	531.4	531.3
		528.0	528.0		528.5	528.4
Li 1s	56.0	56.0	56.0	56.0	56.0	56.0
	55.1	55.0	55.1	54.9	55.0	55.0
	54.1	54.2	54.1		54.1	54.1
F 1s	688.6			688.6		
	684.5	684.4	684.4	684.3	684.4	684.4
	168.4			168.5	168.5	168.5
S 2p	161.0	162.3	162.5	161.0	161.5	161.6
		160.3	160.5	160.0	160.2	160.2
N 1s	398.1	398.1	398.1	398.3	398.5	398.5

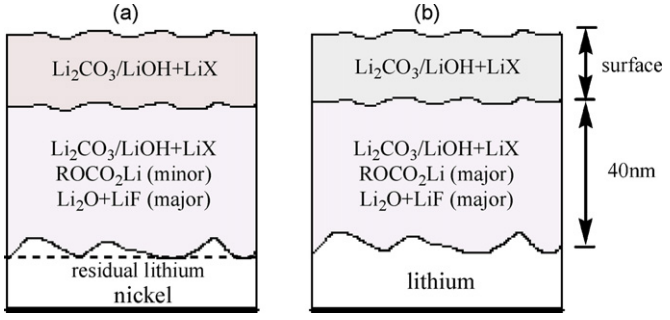

Fig. 5. Schematic illustration for the passive layer formed on lithium in PEO_{20}–LiTFSI–5%PC electrolyte: (a) after Li deposition–dissolution cycle and (b) after Li deposition. LiX: X can be SO_2CF_3, S, N, or F.

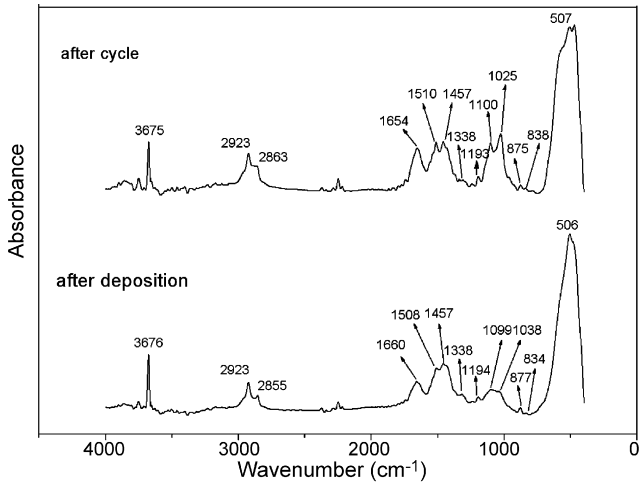

Fig. 6. FTIR spectra of the passive layer obtained from nickel substrate for PEO_{20}–LiTFSI–5%PC electrolyte (transmission mode).

Table 2
Position and assignment for the prominent peaks of the surface film in a PEO\LiTFSI\PC electrolyte

Pos. peak (cm^{-1})		Assignment	Reference(s)
After cycle	After deposition		
507	506	LiO stretch	[21,24]
838	834	CH_2 bend	[21]
875	877	Li_2CO_3	[24–26]
1025	1038	CO stretch	[21]
1100	1099	CO stretch	[21]
1193	1194	CF_3 stretch	[23]
1338	1338	SO_2 stretch	[23]
1457	1457	Li_2CO_3	[24–26]
1510	1508	Li_2CO_3	[24–26]
1654	1660	CO_2 stretch	[21]
2923	2923	CH_2 stretch	[21]
2863	2855	CH_2 stretch	[21]
3675	3676	LiOH	[20,23]

4. Conclusions

In this work, the passive layer formed on lithium in a PEO_{20}–LiTFSI–5%PC gel polymer electrolyte both after Li deposition and after Li deposition–dissolution cycle was characterized using XPS, FTIR, and EIS. The main conclusions are as follows:

(1) XPS and FTIR data show that the composition of the passive layer obtained from the two conditions is basically consistent. This suggested that it has no effect on the composition of the passive layer during lithium dissolution process. PEO seems to be rather inert to lithium, and the passive layer are mainly composed of $ROCO_2Li$, Li_2CO_3 (products of PC reduction), LiOH, Li_2O (products of trace H_2O, O_2) and a

few reduction products of LiTFSI (probably including LiF, Li_2S, Li_3N, $LiSO_2CF_3$, etc.).

(2) Sputtering experiments further demonstrated that Li_2CO_3/LiOH are in the outer layer and Li_2O, LiF mainly in the inner part of the passive layer.

Acknowledgements

We are grateful for financial support from National Natural Science Foundation of China (NNSFC, Grant Nos. 20433060, 20473068 and 29925310) to this work.

References

[1] P.G. Bruce, F. Krok, Solid State Ionics 36 (1989) 171.
[2] D. Fauteux, Solid State Ionics 17 (1985) 133.
[3] M. Hiratani, K. Miyauchi, T. Kudo, Solid State Ionics 28/30 (1988) 1431.
[4] D. Aurbach, I. Weissman, A. Schechter, Langmuir 12 (1996) 3991–4007.
[5] A. Schechter, D. Aurbach, Langmuir 15 (1999) 3334–3342.
[6] V. Eshkenazia, E. Peleda, L. Bursteinb, D. Golodnitskya, Solid State Ionics 170 (2004) 83–91.
[7] K. Kanamura, S. Shiraishi, H. Takezawa, Z. Takehara, Chem. Mater. 9 (1997) 1797–1804.
[8] D. Aurbach, M. Moshkovich, Y. Cohen, A. Schechter, Langmuir 15 (1999) 2947–2960.
[9] D. Aurbach, B. Markovsky, M.D. Levi, E. Levi, A. Schechter, M. Moshkovich, Y. Cohen, J. Power Sources 81/82 (1999) 95.
[10] D. Aurbach, I. Weissman, A. Zaban, O. Chusid, Electrochim. Acta 39 (1994) 51.
[11] E. Peled, D. Bar Tow, A. Merson, A. Gladkich, L. Burstein, D. Golodnitskya, J. Power Sources 97/98 (2001) 52–57.
[12] H. Ota, T. Akai, H. Namita, S. Yamaguchi, M. Nomura, J. Power Sources 119/121 (2003) 567–571.
[13] H. Ota, T. Sato, H. Suzuki, T. Usami, J. Power Sources 97/98 (2001) 107–113.
[14] I. Ismail, A. Noda, A. Nishimoto, M. Watanabe, Electrochim. Acta 46 (2001) 1595–1603.
[15] O. Chusid, Y. Gofer, D. Aurbach, M. Watanabe, T. Momma, T. Osaka, J. Power Sources 97/98 (2001) 632–636.
[16] L.F. Li, D. Totir, Y. Gofer, G.S. Chottiner, D.A. Scherson, Electrochim. Acta 44 (1998) 949–955.
[17] D. Aurbach, M. Daroux, P. Faguy, E. Yeager, J. Electroanal. Chem. 297 (1991) 225–244.
[18] M.A. Vortyntsev, M.D. Levi, A. Schechter, D. Aurbach, J. Phys. Chem. B 105 (2001) 188.
[19] R. Bouchet, S. Lascaud, M. Rosso, J. Electrochem. Soc. 150 (10) (2003) A1385–A1389.
[20] D. Aurbach, M.L. Daroux, P.W. Faguy, E. Yeager, J. Electrochem. Soc. 134 (7) (1987) 1611–1620.
[21] R. Dedryvere, S. Laruelle, S. Grugeon, L. Gireaud, J.M. Tarascon, D. Gonbeau, J. Electrochem. Soc. 152 (4) (2005) A689–A696.
[22] M. Le Granvalet-Mancini, T. Hanrath, D. Teeters, Solid State Ionics 135 (2000) 283–290.
[23] P.C. Howlett, N. Brack, A.F. Hollenkamp, M. Forsyth, D.R. MacFarlane, J. Electrochem. Soc. 153 (3) (2006) A595–A606.
[24] D. Aurbach, J. Electrochem. Soc. 136 (1989) 1611.
[25] K. Morigaki, A. Ohta, J. Power Sources 76 (1998) 159.
[26] J. Li, H. Li, Z.X. Wang, L.Q. Chen, X.J. Huang, J. Power Sources 107 (2002) 1.